ARTICLE NO. 78-982R

J80-182

Analytical Model of High-Pressure Burning Rates in a Transient Environment

60002
60003
60009

Norman S. Cohen* and Leon D. Strand†
Jet Propulsion Laboratory, Pasadena, Calif.

A transient ballistics and combustion model is derived to represent the closed vessel experiment that is widely used to characterize the high-pressure burning rates of solid propellants. The model is applied to show that burning rates deduced from the closed vessel should agree with those measured from an equilibrium strand burner. Thermal profile time lag effects become small at high pressure because the burning rates become high. However, the burning surface structure of those nitramine propellants which exhibit shifts in pressure exponent leads to an anomaly. It is necessary to consider this mechanism in applications dealing with high pressures and pressurization rates.

Nomenclature

A_b = propellant burn surface area, ideal geometry
A_W = surface area of closed vessel wall exposed to heating
c = propellant heat capacity
c_g = gas heat capacity
E_s = activation energy for propellant decomposition
f_{ext} = igniter heat flux, an arbitrary constant
h = depth of surface cratering in nitramine propellants
k = propellant thermal conductivity
m_c = mass of gas in the closed vessel
n = burning rate pressure exponent
P = pressure
$\dot{P}$ = rate of change of pressure
Q_F = gas phase heat of combustion
Q_s = propellant heat of decomposition
Q_W = rate of heat loss to closed vessel wall
$\bar{r}$ = steady-state burning rate at P
r_f = regression rate of binder
$\bar{r}_F$ = steady-state post-break-point burn rate at P
r_i = instantaneous propellant burn rate
r_m = critical burn rate at the exponent break point
$\bar{r}_M$ = steady-state pre-break-point rate at P
r_{ox} = regression rate of nitramine
R = gas constant
R_o = universal gas constant
$(S_{ox}/S_o)_M$ = fraction of exposed nitramine surface on a planar melt surface
$(S_{ox}/S_o)_F$ = fraction of exposed nitramine surface on a cratered surface
$(\overline{S_{ox}})_F$ = value of S_{ox} associated with $\bar{r}_F$
t = time
T = temperature
T_F = propellant adiabatic flame temperature
T_g = instantaneous gas temperature in the closed vessel
T_o = initial (ambient) temperature
T_s = instantaneous propellant surface temperature
$\bar{T}_s$ = steady-state propellant surface temperature associated with $\bar{r}$
T_W = closed vessel wall temperature
V = instantaneous gas volume in the closed vessel
w = propellant web
x = distance from propellant surface into propellant
ϵ = radiation emissivity of gas
η = covolume
γ = ratio of specific heats
κ = propellant thermal diffusivity
ρ = propellant density
σ = Stefan-Boltzmann constant
ξ = steady-state flame height associated with $\bar{r}$ and P (dimensionless)

Introduction

NITRAMINE propellants are of interest for armament and rocket applications because they are an energetic source of combustion products of reduced flame temperature and smoke. Studies in recent years have been devoted to understanding and improving the steady-state combustion characteristics of nitramine propellants, with emphasis upon burning rate control and avoidance of pressure exponent shifts.[1-4] Interest also exists in the time-dependent combustion to the extent that applications encounter high rates of pressure change.[5,6] A question arises as to the effect of a transient pressure environment on the burning of propellants which exhibit exponent shifts, or to what extent a given transient device could tolerate propellants which exhibit exponent shifts.[7,8] This question is addressed in part by the closed vessel (or closed bomb) experiment that is widely used to deduce the high-pressure burning rates of propellants.[9] There has been ongoing work to compare those deduced burning rates with rates measured in an equilibrium strand burner.[10-15] The interest and the experimental results stimulated the analytical work presented in this paper.

Data Synopsis

In the case of homogeneous propellants (unfilled single-based or double-based propellants), there appears to be a general agreement between burning rates as deduced from a closed vessel (transient pressure) and measured from a strand burner (constant pressure). Such was the conclusion of Grollman[13] in a fairly extensive study. Mitchell[14] showed a virtual identity between the closed vessel and strand data, whereas Lenchitz[11] reported the types of small differences published by Grollman. These are typified here by Fig. 1a. On the other hand, there is a significant and consistent difference between closed vessel and strand burning rates in the case of propellants containing HMX which exhibit exponent shifts in

Presented as Paper 78-982 at the AIAA/SAE 14th Joint Propulsion Conference, Las Vegas, Nev., July 25-27, 1978; submitted Aug. 17, 1978; revision received Jan. 16, 1980.

Index categories: Fuels and Propellants, Properties of; Combustion and Combustor Designs; Combustion Stability, Ignition, and Detonation.

*Subcontractor. Member AIAA.
†Member, Technical Staff. Member AIAA.

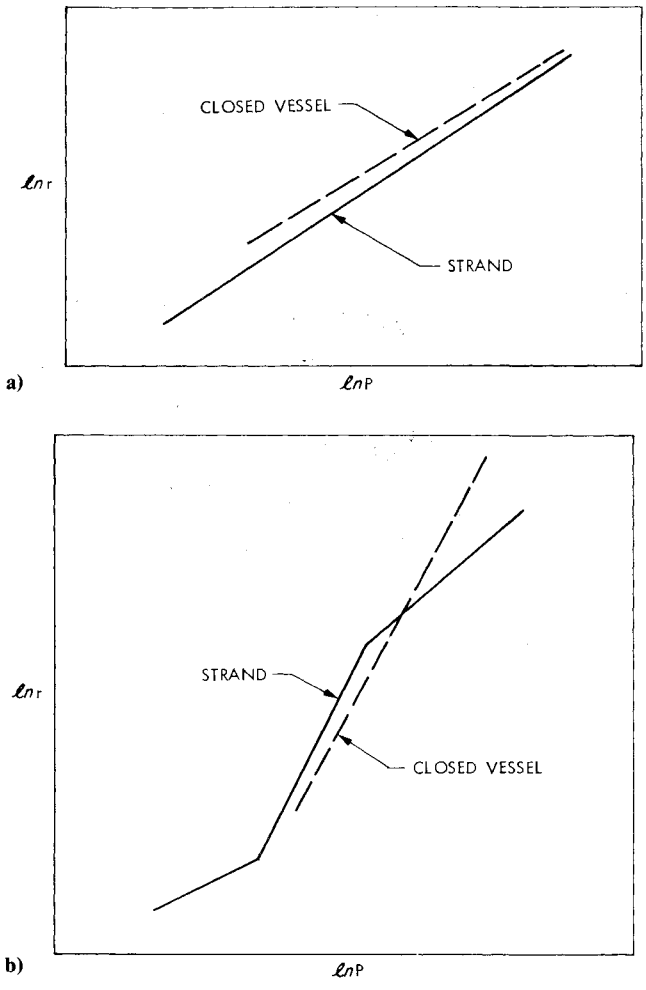

Fig. 1 Typical comparisons of closed vessel and strand burning rates: a) homogeneous propellant, b) nitramine composite propellant.

the strand burner.[10-12] This difference is typified by Fig. 1b. Over the range of pressures reported, the closed vessel data exhibit a more uniform and higher pressure exponent; burning rates appear lower at lower pressures and higher at higher pressures.

Analytical Model

The analytical model for transient combustion is based upon burning surface and flame mechanisms contained within the steady-state model,[1] coupled to a thermal wave relaxation model for a homogeneous solid.[16]

Basic Equations for Thermal Wave Relaxation

Instantaneous burning rate is related to a reference or steady-state value by means of an Arrhenius equation for surface decomposition:

$$r_i = \bar{r}\exp[(-E_s/R_o)(1/T_s - 1/\bar{T}_s)] \tag{1}$$

$\bar{r}$ is known from strand data or the steady-state model. $\bar{T}_s$ is that value from the steady-state model associated with $\bar{r}$. The instantaneous surface temperature is calculated from the time-dependent Fourier equation:

$$\frac{\partial T}{\partial t} = \kappa\frac{\partial^2 T}{\partial x^2} - r_i\frac{\partial T}{\partial x} \tag{2}$$

The initial and in-depth boundary conditions for Eq. (2) are:

$$T(x,0) = T_o \tag{3a}$$

$$\frac{\partial T}{\partial x}(w,t) = 0 \tag{3b}$$

The surface boundary condition is determined from an energy balance based upon the steady-state model.[1] Here, the analysis departs from the models used earlier.[16-18] The surface energy balance is:

$$\kappa\frac{\partial T}{\partial x} + \rho r_i Q_s = \rho r_i Q_F \exp(-\xi) + f_{ext}$$

The second term on the right-hand side represents an igniter heat flux to get the burning under way. It is assumed to be a known quantity. An ignition system per se is not included in the model. The first term on the right-hand side is the heat feedback from the flame. Gas phase processes are assumed to respond in a quasisteady manner. Only one flame is used here—the monopropellant flame. In the case of inert binder nitramine propellants, the diffusion flame becomes unimportant at the high pressures of interest.[1] In the case of active binder propellants, the diffusion flame is taken to be absent because of ingredient stoichiometry.[2] Q_F is eliminated by the surface energy balance in steady-state:

$$\rho c\bar{r}(\bar{T}_s - T_o) + \rho\bar{r}Q_s = \rho\bar{r}Q_F\exp(-\bar{\xi})$$

Combining these equations, and recognizing that ξ is proportional to r^2 at a given pressure,[19] there results:

$$k\frac{\partial T}{\partial x}(0,t) = f_{ext} + \rho r_i\{[c(\bar{T}_s - T_o) + Q_s]\ e^{\xi[1-(r_i/\bar{r})^2]} - Q_s\} \tag{3c}$$

The value of $\bar{\xi}$ is inferred from an overall energy balance:

$$Q_F = c_g T_F - cT_o + Q_s$$

Eliminating Q_F once again, there results:

$$\bar{\xi} = \ell n\left[\frac{c_g(T_F - T_o) + Q_s + (c_g - c)T_o}{c(\bar{T}_s - T_o) + Q_s}\right] \tag{4}$$

The parameters c_g and T_F are functions of pressure, which are accounted for. The foregoing constitute a system of equations for r_i, T_s, temperature gradient, and $\bar{\xi}$, if pressure is known.

Closed Vessel Conservation Equations

The pressure variations are computed by a mass and energy balance for the chamber:

$$(V - \eta m_c)\frac{dP}{dt} = (RT_g + \eta P)\frac{dm_c}{dt} + Rm_c\frac{dT_g}{dt} - P\frac{dV}{dt} \tag{5}$$

$$\frac{dm_c}{dt} = \rho A_b r_i \tag{6}$$

$$\frac{dV}{dt} = A_b r_i \tag{7}$$

$$m_c\frac{dT_g}{dt} = (\gamma T_F - T_g)\frac{dm_c}{dt} - \frac{\dot{Q}_W}{c_g} \tag{8}$$

Equation (5) assumes a constant covolume for the equation of state. The heat loss to the wall is given by:

$$\dot{Q}_W/A_W = h_c(T_g - T_W) + (\epsilon\sigma)_g(T_g^4 - T_W^4) \tag{9}$$

The unsteady heat transfer in the wall may be solved in analogous fashion to Eqs. (2) (with $r_i = 0$) and (3), sub-

stituting Eq. (9) for Eq. (3c) to describe the flux at the wall.

Equations (5-9) constitute five additional equations for P, T_g, m_c, V, and $\dot{Q}_w$. The overall system of nine equations is sufficient for a homogeneous propellant. Additional equations, to be presented subsequently, are required to complete the description for nitramine propellants. These equations are solved numerically by a forward difference method.[16] The instantaneous burning rate will differ from the steady-state value at a given pressure to the extent that T_s differs from $\bar{T}_s$.

Surface Structure Effects in Nitramine Propellants

Additional equations enter into the system for nitramine propellants because of the relationship of the surface structure to the burning rate.[1] It is assumed that the surface structure will develop in three stages in the course of the pressurization transient: 1) formation of the melt layer following ignition, 2) disappearance of the melt layer when the exponent shift or break point criterion[1] is reached, and 3) formation of the surface craters following disappearance of the melt layer.

The melt layer will start to form as soon as $T_s = T_M$, the melting point of the nitramine. It is expected that the location of T_M will move into the solid with time; T_M is 551 K for HMX, and computed steady-state surface temperatures are circa 1000 K. The melt layer thickness, located by T_M, is monitored during this first stage. The second stage commences when the critical burning rate[1] is exceeded, $r_i > r_m$, such that subsurface melting can no longer propagate. At this time step, the endothermic heat of fusion component of Q_s[1] is set to zero, and the existing melt layer thickness is allowed to decompose away in accordance with the time integral of r_i in succeeding time steps. This stage is completed when the melt layer has disappeared. The formation of craters during the third stage necessitates additional relations.

From the steady-state model, it is known that the area change from $(S_{ox}/S_o)_M$ to $(S_{ox}/S_o)_F$ is the essential manifestation of the exponent break point wherein $\bar{r}$ jumps from a value influenced by the binder to a value close to the nitramine monopropellant rate.[1] Therefore, in the course of the break point transition, it may be assumed that $\bar{r}$ is proportional to the change in (S_{ox}/S_o). This assumption is made in order to avoid jump discontinuities in the time-dependent model, and to allow smooth (continuous) transition. Further, it is anticipated that the break point in the time-dependent model need not occur at the same pressure as in the steady-state model. That is, the pressures for $r_i > r_m$ and $\bar{r} > r_m$ may be different. Thus, it is necessary to consider values of $\bar{r}$ which extrapolate pre-break-point planar surface rates ($\bar{r}_M$) to higher pressure, and post-break point cratered surface rates ($\bar{r}_F$) to lower pressure. If the cratering actually occurs at some different pressure than steady-state, a proper value of $\bar{r}$ may still be used in accordance with the surface existing at the time. Equation (1), as applied during this third stage of surface development, then becomes:

$$\frac{r_i}{\bar{r}_M} = \exp[(-E_s/R_o)(1/T_s - 1/\bar{T}_s)] \times \left\{1 + \left[\frac{\bar{r}_F}{\bar{r}_M} - 1\right]\left[\frac{(S_{ox})_F - (S_{ox})_M}{(S_{ox})_F - (S_{ox})_M}\right]\right\} \tag{10}$$

Relations for $(S_{ox}/S_o)_M$, $(S_{ox}/S_o)_F$, and r_m are provided by the steady-state model.[1] The functions $\bar{r}_M(P)$, $\bar{r}_F(P)$, their extrapolations, and the location of the break point in steady-state may be acquired from steady-state model calculations or examination of strand data. For transient calculations, the use of strand data is preferred to avoid errors from the steady-state model. Use of the steady-state model is limited to obtaining values of $\bar{T}_s$ and $(S_{ox}/S_o)_F$. The parameter $(S_{ox}/S_o)_F$ changes with time because the cratering penetration depth h changes with time.[1] The variation of the penetration depth with time is expressed as follows:

$$dh = (r_{ox} - r_f)\,dt \tag{11}$$

Relations for r_{ox} and r_f are provided by the steady-state model,[1] and depend upon whether or not the binder is a monopropellant.[2]

Model Results

Homogeneous Propellant Test Case

The homogeneous propellant test case selected for model validation was "test propellant A" as specified by the referenced JANNAF Workshop.[15] Burning rates were reported by six different laboratories for a given set of specifications and closed vessel pressure-time data. However, the identity of the propellant was not disclosed and strand burning rates were not given. In the absence of strand data, the reported burning rates were used as baseline equilibrium data for purposes of model application. The data were reported over the pressure range 34-272 MPa. An average of the results for the six laboratories was used at each pressure, and an extrapolation was performed to complete the input down to ambient pressure. Although these data are closed vessel data, the model would still be useful to show the effect of the closed vessel environment, if any. If such effect is small, as expected, the model should reproduce these data as well as the measured pressure-time curve.

The burning rate results are shown in Fig. 2. The solid line represents the actual closed vessel data, except for pressures below 34 MPa where it is an extrapolation. The model prediction is represented by the circles. It is observed that the prediction is very close to the line between 34 and 272 MPa, indicating a very small effect of the transient environment.

An interesting undulation appears in the predicted results between 27 and 82 MPa. Similar undulations have been noted in previous analyses.[18] The interpretation involves the competing processes of surface heating and transpiration cooling during the pressure rise,[18] and the effect increases with increasing Q_s and decreasing $\bar{r}$. The undulations dampen as $\bar{r}$ increases.

The most interesting behavior appears at low pressure. The very high initial burning rates are largely a consequence of the

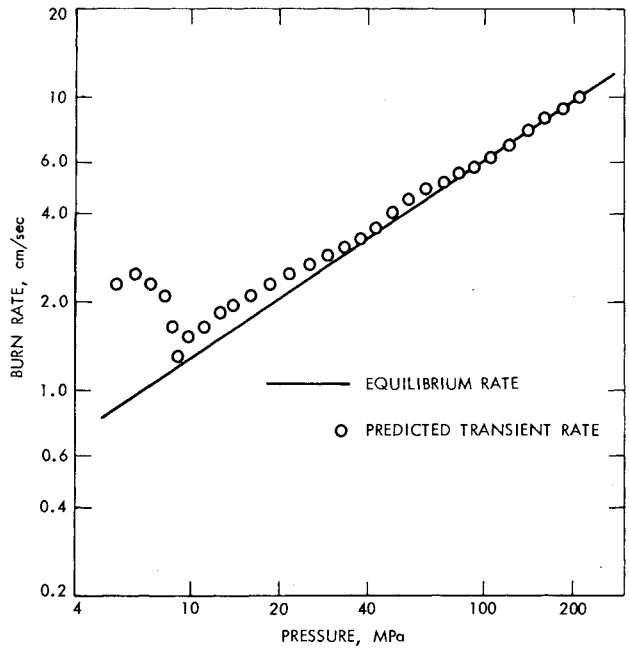

Fig. 2 Predicted effect of closed vessel environment on burning rate of homogeneous propellant.

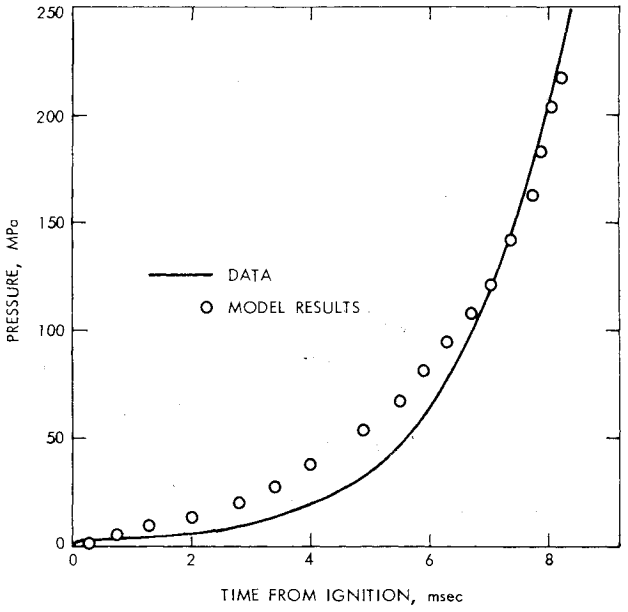

Fig. 3 Comparison of predicted and experimental pressurization for test corresponding to Fig. 2.

assumed igniter. If this arbitrary heat flux remains operative during burning and is large compared to the combustion-induced heat flux, the burning rate will be high. The igniter is turned off at 6.8 MPa, and the burning rate immediately drops because the transpiration cooling becomes excessive for the remaining heat imposed. The burning rate climbs again when the transient heating is re-established. Here, then, is a second type of burning rate undulation. A third type (not shown here) results from preignition thermal soak of the propellant,[16] or dynamic "overshoot" due to a sudden imposed compression.[17] Thus, there are mechanistic bases for low-pressure burning rate undulations, depending upon the nature of the ignition process and developing combustion-induced heating. These effects, although real, are undesirable for purposes of closed vessel data acquisition and are lumped into the area of uncertainties. As a result, burning rates deduced from the closed vessel generally exclude results below 34 MPa. An accurate quantification of the low-pressure behavior would require a model of the igniter.

Predicted pressure-time results are shown together with the Workshop furnished data in Fig. 3. Time is measured from ignition time rather than zero time to remove the differences in ignition delay and afford a better visual comparison. Initial pressurization is overpredicted because of the effect of the assumed igniter. This also causes the predicted web to advance relative to the actual web at a given time and pressure. The curves then merge and the prediction becomes very good at the higher pressures. The pressure results are consistent with the burning rate results.

Nitramine Propellant Test Case

The nitramine propellant test case selected for model validation is the 92-μm HMX propellant reported by Lenchitz.[11] Much of the required input information is contained within that paper, including actual strand burning rate data to serve as the equilibrium baseline. The paper also reports the pressurization history for that test.

The burning rate results are shown in Fig. 4. Plotted are the strand data (solid line), deduced closed vessel data (solid circles), and the predicted actual (open circles) burning rates in the closed vessel.

In the region below 14 MPa, much the same behavior appears as was discussed for the homogeneous propellant; the burning rate is first dominated by the behavior of the assumed igniter and then drops when the igniter is turned off. Note,

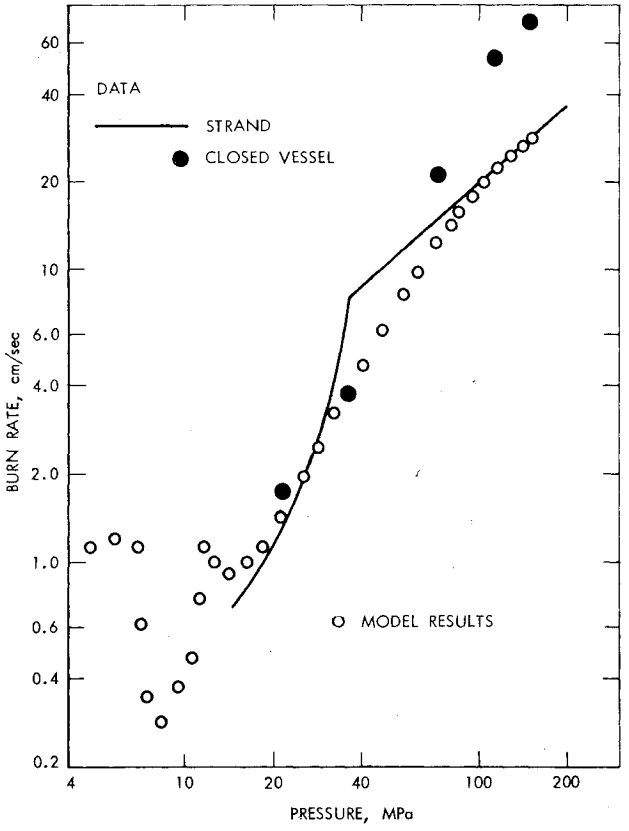

Fig. 4 Predicted and experimental effects of closed vessel environment on burning rate of nitramine propellant.

however, the appearance of a second burning rate undulation just below 14 MPa. This is a consequence of a fourth mechanism for undulation and will be unique to nitramine propellants which exhibit an exponent shift. According to the model, an exponent break point is being traversed, causing a greater burning rate than can momentarily be sustained by the combustion heating then in existence. The rate falls until sufficient heating develops to resustain it. If the rate fell to the extent that the surface melt layer would reform, then an endotherm would reappear to drop the rate further; such a process might appear as a fifth type of undulation. No data were reported below 14 MPa, but the model results are not expected to be accurate in that regime because the igniter is not modeled.

The region between 14 and 68 MPa is interesting because it shows how the predicted actual burning rates in the closed vessel differ from equilibrium data. Basically, the post-break-point surface structure cratering of the propellant is developing gradually in the course of the transient in the closed vessel. This continuous development lags the equilibrium cratering at each discrete test-to-test pressure level in the strand burner. At pressures above 68 MPa, the predicted actual burning rates in the closed vessel approach the equilibrium strand data as the surface structure becomes more fully developed.

The predicted burn rate does not depart significantly from the experimentally deduced burn rate until pressures are in excess of 60 MPa. Over the range 20-60 MPa, the predictions are generally on the low side, but agree rather well with the data. Thus, it is concluded that the high (closed vessel) burn rates at high pressure, relative to the strand data, are due entirely to a surface area effect and not a transient burn rate effect. A cratered surface structure can eventually lead to grain breakup in small grains near burn-out, which would provide increased area.

The predicted pressurization is compared with data in Fig. 5. Here, the data were reported as rate of change of pressure

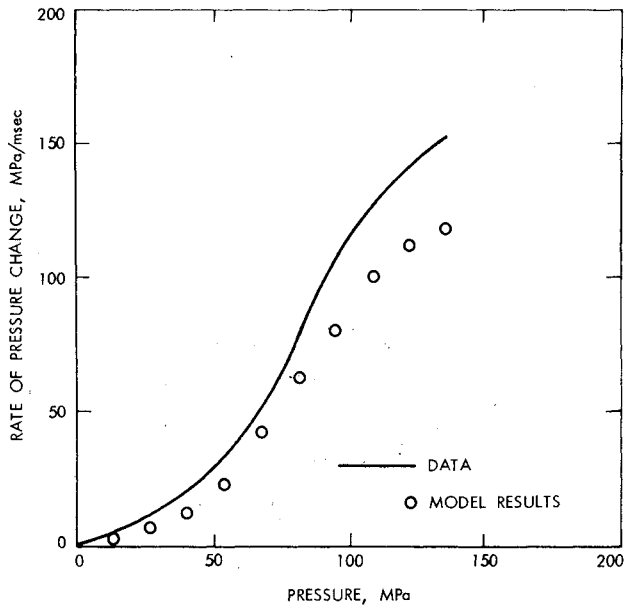

Fig. 5 Comparison of predicted and experimental pressurization for test corresponding to Fig. 4.

vs pressure rather than as pressure vs time. This is a more severe test of the model because a number of factors enter into the rate pressure change at a given pressure. The prediction falls below the data, which is consistent with the underprediction of the mass generation rates, but the agreement is rather good considering all of the factors involved.

Based upon the results of this effort and the steady-state modeling effort, it would be expected that closed vessel burning rates should agree with strand burning rates when the HMX particle size is sufficiently fine that there is no surface cratering. This is borne out by results with 4μ HMX.[11] For that propellant, there was no exponent shift and the closed vessel rate agreed with the strand rates. On the other hand, with a 45μ HMX propellant, a sharp exponent break appeared in the strand data and the composite data plot was qualitatively identical to Fig. 4.[11]

Conclusions

Burning rate data and model calculations indicate that, at high pressures, thermal wave relaxation processes have but a small effect upon burning rates under transient pressure conditions encountered in the typical closed vessel experiment. Thus, burning rates derived from the closed vessel and equilibrium strand burner should substantially agree. In nitramine propellants containing sufficiently coarse powder, the development of a cratered surface structure will cause apparent burning rates in a transient device to differ from the actual rates near burn-out.

At low pressures, thermal wave relaxation pressures will produce apparent anomalies such as nonlinear combustion oscillations. Accurate description of the low-pressure interior ballistics of a particular device will require a model of the igniter because of the impact upon the transient pressure and combustion energy balance.

Acknowledgment

This work was sponsored by the Air Force Office of Scientific Research under Contract AFOSR-ISSA-77-0001, through an agreement with NASA. The authors express their appreciation to C. F. Price of the Naval Weapons Center for helpful discussions regarding the closed vessel experiment and the computer programming of the model.

References

[1] Cohen, N. S. and Price, C. F., "Combustion of Nitramine Propellants," *Journal of Spacecraft and Rockets,* Vol. 12. Oct. 1975, pp. 608-612.

[2] Cohen, N. S. and Strand, L. D., "Nitramine Propellant Research," Rept. AFOSR-TR-76-1163, JPL TM 33-801, Jet Propulsion Laboratory, Pasadena, Calif., Oct. 1976.

[3] McCarty, K. P., Beckstead, M. W., and Simmons, R. L., "HMX Propellant Combustion Studies," Rept. AFRPL-TR-76-59, Hercules Inc., Magna, Utah, Dec. 1976.

[4] Simmons, R. L., "Workshop Report: Nitramine Gun Propellant Combustion," *13th JANNAF Combustion Meeting*, CPIA Publication 281, Vol. I, Dec. 1976, pp. 1-8.

[5] Price, E. W., Coordinator, ONR-AFOSR Workshop on Deflagration-to-Detonation Transition, Atlanta, Ga., Jan. 1978.

[6] Heiney, O. K., Coordinator, TTCP Panel W-4 KTA-6 Gun Propellant Meeting, Air Force Armament Laboratory, Eglin AFB, Fla., March 1978.

[7] Heiney, O. K., AFOSR-AFATL Explosive Combustion Meeting, Eglin AFB, Fla., April 1974.

[8] Rocchio, J. J., et al., "Results of Recent Experimental and Theoretical Studies of Nitramine Gun Propellant Performance," *13th JANNAF Combustion Meeting*, CPIA Publication 281, Vol. I, Dec. 1976, pp. 9-19.

[9] Boggs, T. L. and Lenchitz, C., Coordinators, JANNAF Workshop on Burning Rate Measurements, Calculations and Data Reduction Production Procedures, Ballistics Research Laboratories, Aberdeen Proving Ground, Md., Oct. 1976.

[10] Derr, R. L., AFOSR-AFATL Explosive Combustion Meeting, Eglin AFB, Fla., April 1974.

[11] Lenchitz, C., "The Role of Thermochemistry in HMX Propellant Burning," *12th JANNAF Combustion Meeting,* CPIA Publication 273, Vol. II, Dec. 1975, pp. 301-321.

[12] Price, C. F., private communications, Ballistics Research Laboratories, Aberdeen Proving Ground, Md., 1976.

[13] Grollman, B. B. and Nelson, C. W., "Burning Rates of Standard Army Propellants in Strand Burner and Closed Vessel Tests," *13th JANNAF Combustion Meeting*, CPIA Publication 281, Vol. I, Dec. 1976, pp. 21-43.

[14] Mitchell, S. E. and Horst, Jr., A. W., "Comparative Burning Rate Study," *13th JANNAF Combustion Meeting*, CPIA Publication 281, Vol. I, Dec. 1976, pp. 383-404.

[15] Boggs, T. L. and Lenchitz, C., Memoranda issued pursuant to the JANNAF Workshop on Burning Rate Measurements, Calculations, and Data Reduction Procedures, Ballistics Research Laboratories, Aberdeen Proving Ground, Md., 1977.

[16] Cohen, N. S., "Ballistic Predictions for Mass-Augmented Solid Rocket Motors," Rept. AFRPL-TR-71-133, Lockheed Propulsion Co., Dec. 1971.

[17] Krier, H., T'ien, J., Sirignano, W., and Summerfield, M., "Nonsteady Burning Phenomena of Solid Propellants," *AIAA Journal*, Vol. 6, Feb. 1968, pp. 278-285.

[18] Kooker, D. E. and Nelson, C. W., "Numerical Solutions of Three Solid Propellant Combustion Models During a Gun Pressure Transient," *12th JANNAF Combustion Meeting*, CPIA Publication 273, Vol. I, Dec. 1975, pp. 173-197.

[19] Beckstead, N. W., Derr, R. L., and Price, C. F., "A Model of Solid Propellant Combustion Based on Multiple Flames," *AIAA Journal*, Vol. 1, Dec. 1970, pp. 2200-2207.